GSA DATA REPOSITORY 2015271

Appendix DR1. Sample selection criteria, lithology classes, support vector machine classifier, oceanographic datasets, Figures DR1-DR8, Tables DR1-DR2

Census of Seafloor Sediments in the World's Ocean Basins

Adriana Dutkiewicz*, R. Dietmar Müller, Simon O'Callaghan and Hjörtur Jónasson
*correspondending author: adriana.dutkiewicz@sydney.edu.au

METHODS AND DATASETS

Sample selection criteria and lithology classes

We selected 14,399 data points from the total number of 202,000 (as of November 2014) available through the Index to Marine and Lacustrine Geological Samples (IMLGS) (Curators of Marine and Lacustrine Geological Samples Consortium, 2014) using strict quality-control criteria. For areas with poor sample coverage, our dataset was supplemented by descriptions acquired from non-participating agencies such as Geoscience Australia (Passlow et al., 2005). Trawl samples were not used as they represent mixed material whose exact location is unknown. We did not use dredge samples as these usually sample rock rather than overlying soft sediment and represent a sampling bias. Only surface or near-surface (decimeters below surface) samples were used that were collected using coring, drilling or grabbing methods. Deep-sea sediment sampling methods, including box coring (Barnett et al., 1984) can result in mechanical disturbance of soft sediment. This may include sediment loss, sediment flow-in and the formation of new deformation structures such as contorted bedding (Skinner and McCave, 2003). These disturbances are most severe in non-cohesive sandy sediments with cohesive clayey facies remaining relatively undisturbed (Jutzeler et al., 2014). We cannot completely exclude the possibility that some of our sediment descriptions are derived from cores that may be disturbed or missing tops (Stow and Aksu, 1978), but based on original descriptions we have been able to discard the most extremely affected samples from our dataset. However, sediment disturbance is often difficult to recognize (Jutzeler et al., 2014) and unless severe its occurrence is often omitted from original cruise reports. Additionally, the absence of good quality core photographs in most of the cruise reports prevented us from making our own assessment of core disturbance. For the purpose of the lithology map, the quality of the sediment core is not critical as long as the overall composition of the youngest sediment is representative of the sediment at the seafloor. Even if several cm or dm of sediment are missing from some of the core tops in our dataset, if we consider that biogenic oozes have average sedimentation rates of 1 cm/ka (Trujillo and Thurman, 2014), but may be as high as 20 cm/ka (Scholle et al., 1983) and that oceanographic conditions are unlikely to have changed dramatically over that time period, then the lithology preserved at several dm below the seafloor is

representative of the material at the seafloor. Any potential errors in this extrapolation are further diluted by the composition of multiple near-neighbor samples and the gridding algorithm.

Although the IMLGS contains sediment classifications for many samples, these are generic and ambiguous (e.g., “terrigenous mud or ooze”) preventing the sediment from being correctly classified. Consequently, we only used samples whose descriptions could be verified using original cruise reports, cruise proceedings and core logs. In addition, these descriptions had to be sufficiently detailed to allow classification into one of our designated groupings. For example, if the sediment were simply described as mud or ooze in the original report without any other information, it was not used. Because we have a relatively small number of points from the continental shelf, we have mostly concentrated our efforts on the deep sea. Areas of the map with limited sample coverage (e.g., parts of the Southern Ocean, the South Pacific, the Arctic Ocean and the East China Sea) indicate lack of sampling, unavailability of cruise reports and hence lack of reliable sample descriptions. Seafloor in the northern hemisphere has been much more densely sampled than in the southern hemisphere as illustrated by the coordinates of the sample locations in the IMLGS (Curators of Marine and Lacustrine Geological Samples Consortium, 2014); 85% (not normalized to account for larger area of Southern Ocean seafloor) are from the northern hemisphere. This sampling asymmetry is consistent with spatial analysis of distribution of marine survey tracks (Wessel and Chandler, 2011).

The lithology classes on our seafloor sediment map are defined below and include various sediment types based on descriptions from cruise reports and logs:

Gravel: unconsolidated sediments coarser than sand; includes gravel, shelly gravel, sandy gravel, muddy gravel, pebbles, cobbles, diamicton, erratics, rock fragments, loose conglomerate, ice-rafted exotics, and till.

Sand: unconsolidated sediment dominated by sand-sized grains; includes quartz sand, detrital sand, shelly sand, glauconitic sand, clastic sand, silty sand, muddy sand, bioclastic sand, clayey sand, and clayey shelly sand.

Silt: unconsolidated sediment dominated by silt-sized grains; includes diatomaceous silt, clayey silt, sandy silt, calcareous silt, muddy silt, lutaceous silt, and shelly sandy silt.

Clay: unconsolidated sediment dominated by a clay-sized fraction and characterized by low carbonate and low biogenic content; includes sediments variously described as lutite, red clay, brown clay, zeolitic clay, zeolitic red clay, hemipelagic clay, pelagic clay, lutaceous clay, biosiliceous clay, radiolarian clay, diatomaceous clay, foraminiferal clay, radiolarian clay, foram lutite, silty clay, palagonitic clay, ashy clay and manganese lutite.

Diatom ooze: unconsolidated sediment containing > 30% diatom skeletons, in which diatoms are the dominant biogenic component; includes sediments variously described as diatom clay, clayey diatom ooze, diatomite, diatom mud, muddy diatom ooze, diatom clay ooze, diatom silty clay, radiolarian diatom ooze, and diatom marl.

Radiolarian ooze: unconsolidated sediment containing > 30% radiolarian skeletons, in which radiolarians are the dominant biogenic component; includes radiolarite.

Sponge spicules: unconsolidated sediments containing > 30% sponge spicules; includes spiculite.

Calcareous ooze: unconsolidated sediment containing > 30% calcareous skeletons (foraminifera, pterapods, coccoliths); includes sediments described as chalk if biogenic content is > 30%, calcareous marly ooze, foraminiferal marly ooze, foraminiferal chalk, chalk ooze, clayey nanno ooze, foraminiferal sand, foraminiferal marl and calcilutite if foraminifera > 30%.

Mixed calcareous-siliceous ooze: unconsolidated sediment containing > 30% of approximately equal portions of calcareous and siliceous microfossils. Proportions of these are often not specified in original reports or logs and sediment is simply classified as calcareous-siliceous ooze. Biogenic material includes foraminifera, nannofossils, discoasters, pteropods, diatoms, radiolarians and sponge spicules.

Shells and coral fragments: unconsolidated sediment dominated by biogenic fragments that are not oozes; includes shell hash, coral fragments, bryozoan fragments, reef sand, skeletal debris, coral hash, calcareous sand with minor terrigeous content, Halimeda fragments, coral hash, reef debris, limestone fragments, shells and mollusc fragments.

Transitional calcareous sediments: unconsolidated calcareous sediment containing < 30% identifiable biogenic components; includes marl, foraminiferal marl, radiolarian marl, calcareous clay, calcareous mud, calcilutite, nanno clay, foraminiferal clay/lutite, chalk if biogenic content is < 30%, mixtures of calcareous and siliceous clays, mixtures of terrigenous and calcareous clay.

Transitional siliceous sediments: unconsolidated siliceous sediment containing no or low amounts of carbonate including sediments described as mud, terrigenous mud, sandy mud, silty mud, sandy clay, sandy lutite, clayey mud and diatom mud (diatoms < 30% of sediment; if diatom mud contains > 30% diatoms, it is classified as diatom ooze).

Volcaniclastics: any unconsolidated sediment in which volcaniclastic grains are dominant irrespective of grain-size; includes ash, clayey ash, lapilli, glass, volcanic sand, volcanic mud, volcanic gravel, volcanic breccia, vitric silt, tuff, palagonite, tephra, silty tephra and volcanogenic detritus.

Support Vector Machine Classifier

A Support Vector Machine (SVM) (Cortes and Vapnik, 1995) is a classifier that attempts to separate classes of data mapped to a space where it can be separated by a hyperplane. The location of the plane in the input space is selected based on a set of training examples, $x_i \in \Re^d$ $(i = 1, 2, \ldots \ldots, N)$, labeled with a binary variable, $y_i \in \{-1, 1\}$. To

query the label of a new point, the algorithm simply determines on which side of the plane the point sits, $\mathrm{sgn}[f(x)]$ where $f(x)$ represents the discrimant function associated with the hyperplane

$$f(x) = w\phi(x) + b \qquad (1)$$

Here, w, $\phi(\cdot)$ and b denote the weight vector, the basis function and the bias term, respectively. In two dimensions, this amounts to dividing the input space into two sections with a straight line. Typically however, the input data are not linearly separable in their original space and so they are projected into a higher space using a kernel function to produce more flexible decision boundaries in the low dimensional input space. The parameters of this kernel function dictate the type of projection and consequently the behavior of the decision boundaries. The SVM's ability to naturally adjust the complexity of boundaries if the data suggests a more elaborate underlying process is a key reason as to why it is often favored over more rigid classifiers such as random forests (Liaw and Wiener, 2002). Learning the parameter values, which optimize the classifier's performance on withheld data is an important step in the workflow.

The SVM in this paper was trained using five-fold cross-validation. The key parameters, C (which controls the penalty incurred by the model for ignoring misclassified points) and γ (a parameter of the SVM's kernel function), were optimized to maximize the model's predictive power on observations that were held-out during training. The final values employed for the results presented were $C = 3.16$ and $\gamma = 0.1$. A sensitivity analysis plot is included in Fig. DR2 illustrating the behavior of the classifier's cross-validation accuracy as these key parameters were varied. The yellow circular marker indicates the final set of parameters used by the model (Fig. DR2).

To handle the multi-label nature of the data, a one-versus-one approach was adopted. A separate SVM was trained for each pair of labels resulting in $L(L-1)$ different classifers, where L is the number of labels. During prediction, each classifier was evaluated at the query location and the most frequently returned label was used as the model's output.

The accuracy of the SVM classifier is illustrated in Figs DR3 and DR4. Deep-sea lithologies (diatom oozes, calcareous oozes and clay) that collectively comprise over 70% of seafloor sediment (Table DR1) have been predicted with very high accuracy (up to 80%). Minor misclassifications of radiolarian ooze as clay, and that of transitional classes such as mixed calcareous-siliceous ooze and fine-grained calcareous sediments as calcareous ooze are due to a compositional overlap and physical proximity of these lithologies. This has not affected the veracity of the final gridded map (Fig. 2). It is also common for a rare lithology (e.g., gravel and shells) to be misclassified as a common lithology simply due to the large difference between their likelihoods of occurrence (Fig. DR3).

Oceanographic Datasets

Datasets of sea-surface temperature, salinity, dissolved oxygen and dissolved inorganic nutrients (nitrate, phosphate, silicate) (Antonov et al., 2010; Garcia et al., 2010a; Garcia et al., 2010b; Locarnini et al., 2010) were accessed from the World Ocean Atlas 2009 at http://www.nodc.noaa.gov/OC5/WOA09/woa09data.html between August 2014 and January 2015. The data used represent objectively analyzed means at 1° grid resolution.

The surface productivity dataset based on Sea-viewing Wide Field-of-view Sensor (SeaWiFS) r2010 reprocessing results was obtained from http://orca.science.oregonstate.edu/1080.by.2160.monthly.hdf.vgpm.s.chl.a.sst.php in January 2015. We calculated summer month averages (periods of maximum phytoplankton productivity) for the Northern Hemisphere (June, July, August) and Southern Hemisphere (December, January, February) for the period 1997-2009.

Bathymetry data were obtained in November 2014 from ETOPO1 Global Relief Model (Amante and Eakins, 2009) at http://www.ngdc.noaa.gov/mgg/global/global.html.

Although diatom blooms are enhanced by iron fertilization (Denman, 2008) certain open-water species have adapted their photosynthetic apparatus to require less iron (Strzepek and Harrison, 2004) resulting in thicker and heavier frustules (Hutchins and Bruland, 1998). However, we were unable to explore the impact of iron concentrations on preserved lithologies as the data coverage is relatively poor and biased towards the northern hemisphere (Moore and Braucher, 2008). Large intra-basin variabilities that are known to exist (Boyd and Ellwood, 2010) would invariably lead to substantial gridding errors, particularly in the Southern Ocean high-nutrient low-chlorophyll (HNLC) region. The Southern Ocean receives very little iron from eolian dust (Jickells et al., 2005) and other sources (e.g., from continental margins) have not been quantified.

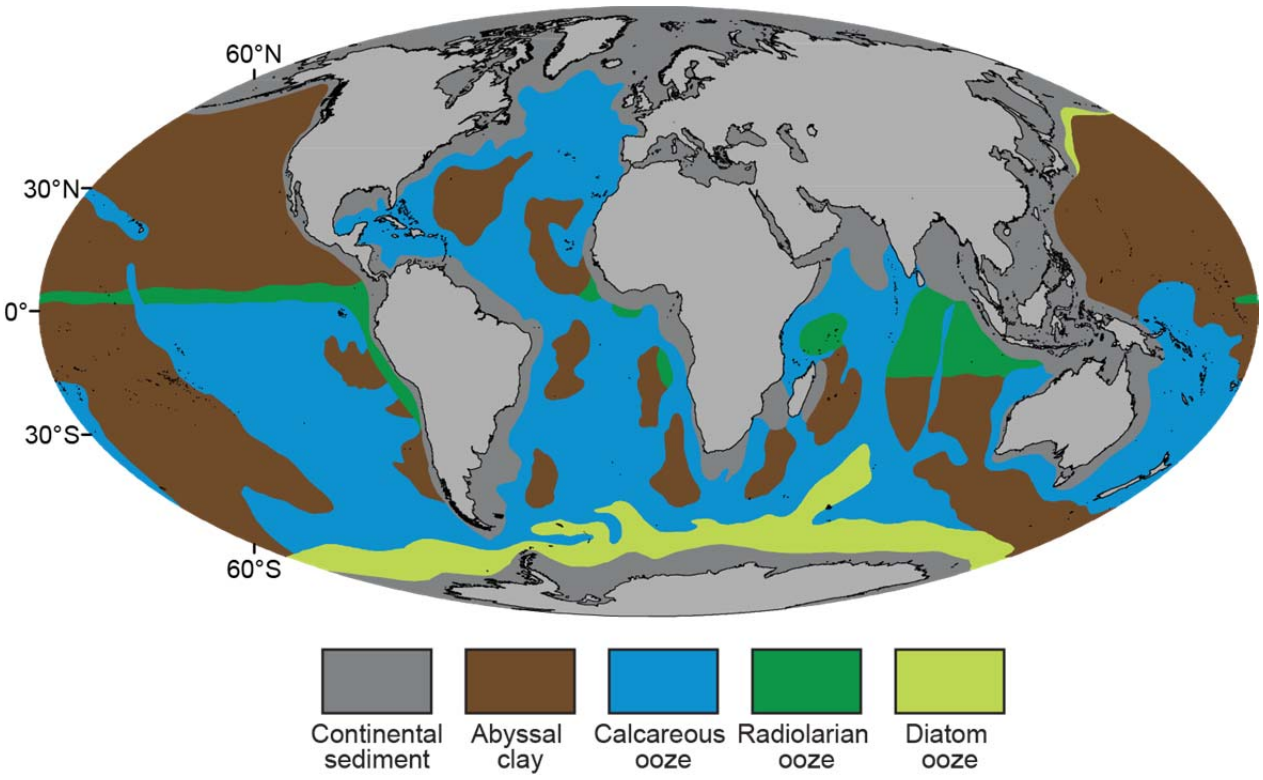

Figure DR1. A typical example of a map showing the distribution of deep-sea sediments in the world's oceans. Color scheme is the same as in Figs 1 and 2. Mollweide equal-area projection. Modified after Trujillo and Thurman (2014). This hand-drawn map has remained unchanged since 1983 and is based on the Deck41 data (Bershad and Weiss, 1974) supplemented by ODP data (Trujillo, A.P., pers. comm., October 2014).

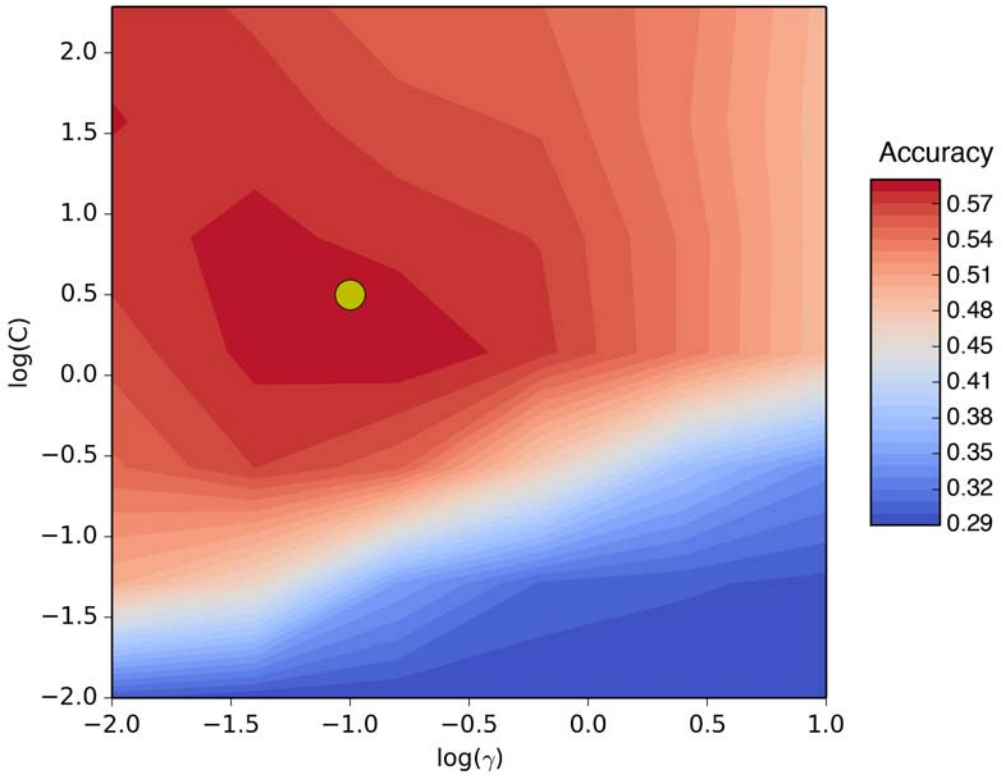

Figure DR2. Sensitivity analysis plot for the SVM classifier's two key parameters, C and γ. Accuracy was evaluated using 5-fold cross-validation. Yellow circular marker indicates final set of parameters used by the model. C controls the penalty that the model receives for misclassifying a point. For a small C, the model will favor smoother interpolations of that data; this is because it is rewarded for choosing the simplest model possible. However, for a large C the penalty for misclassifying begins to have a stronger influence than the reward for a simple model and so the SVM will prefer a complex model that fits the data well but generalizes poorly. In terms of γ, a smaller γ terms give rise to more complex models, which generalize poorly but fit the training data while larger γ terms produce simpler models and generalize well at the risk over being too smooth. The cross validation step is designed to strike a balance between fitting the data and performing well on data that was withheld from the model.

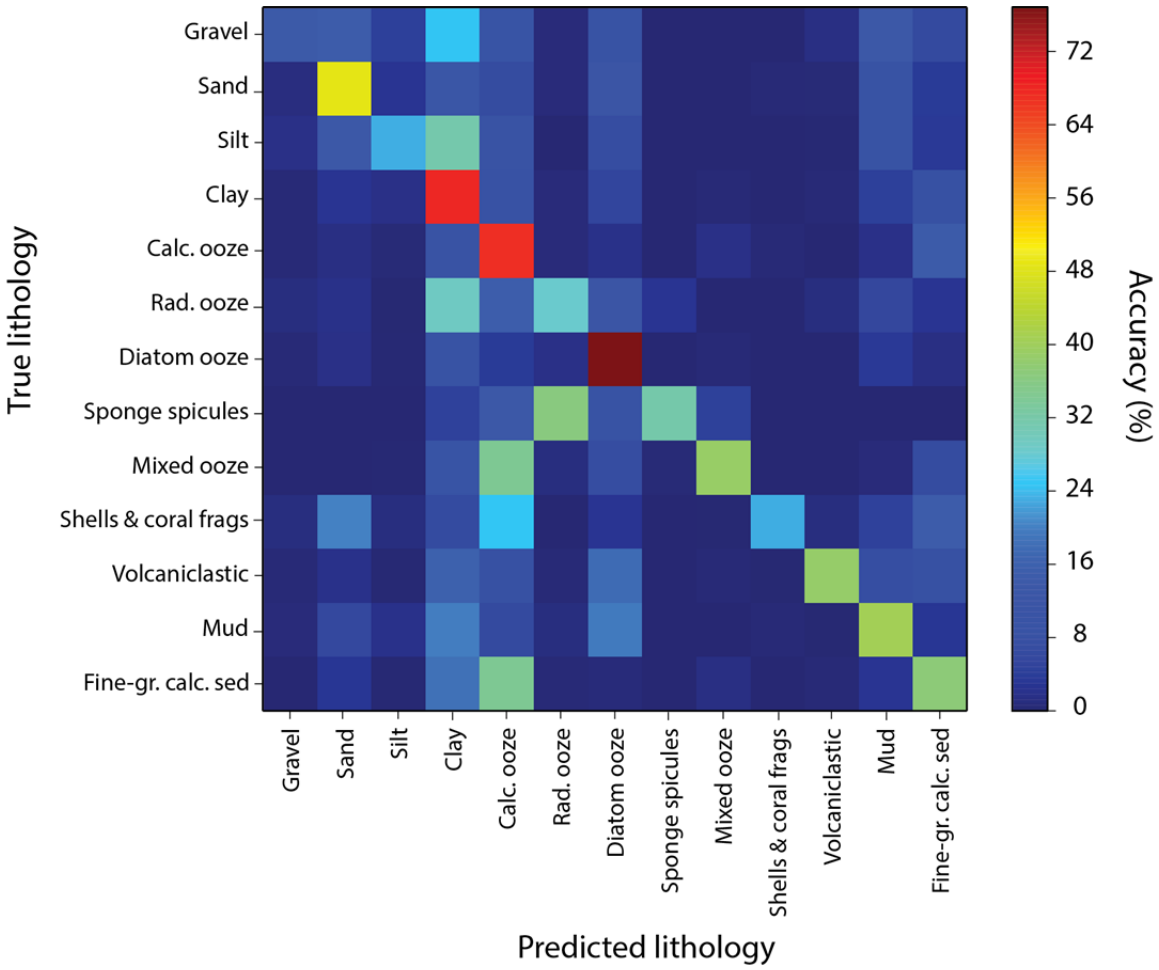

Figure DR3. Confusion matrix for the digital seafloor lithology map. The matrix illustrates the support vector classifier's accuracy in predicting lithology in our dataset. Each row corresponds to a distribution over the algorithm's prediction on a class label (lithology type) that was withheld during the model's training phase. In the case where the classifier is 100% accurate at predicting each lithology, the matrix would be a diagonal one. The more red the diagonal boxes of the matrix, the higher the number of points for which the true lithology has been correctly predicted. Off-diagonal values correspond to a number of points whose lithology has been incorrectly predicted by the support vector classifier.

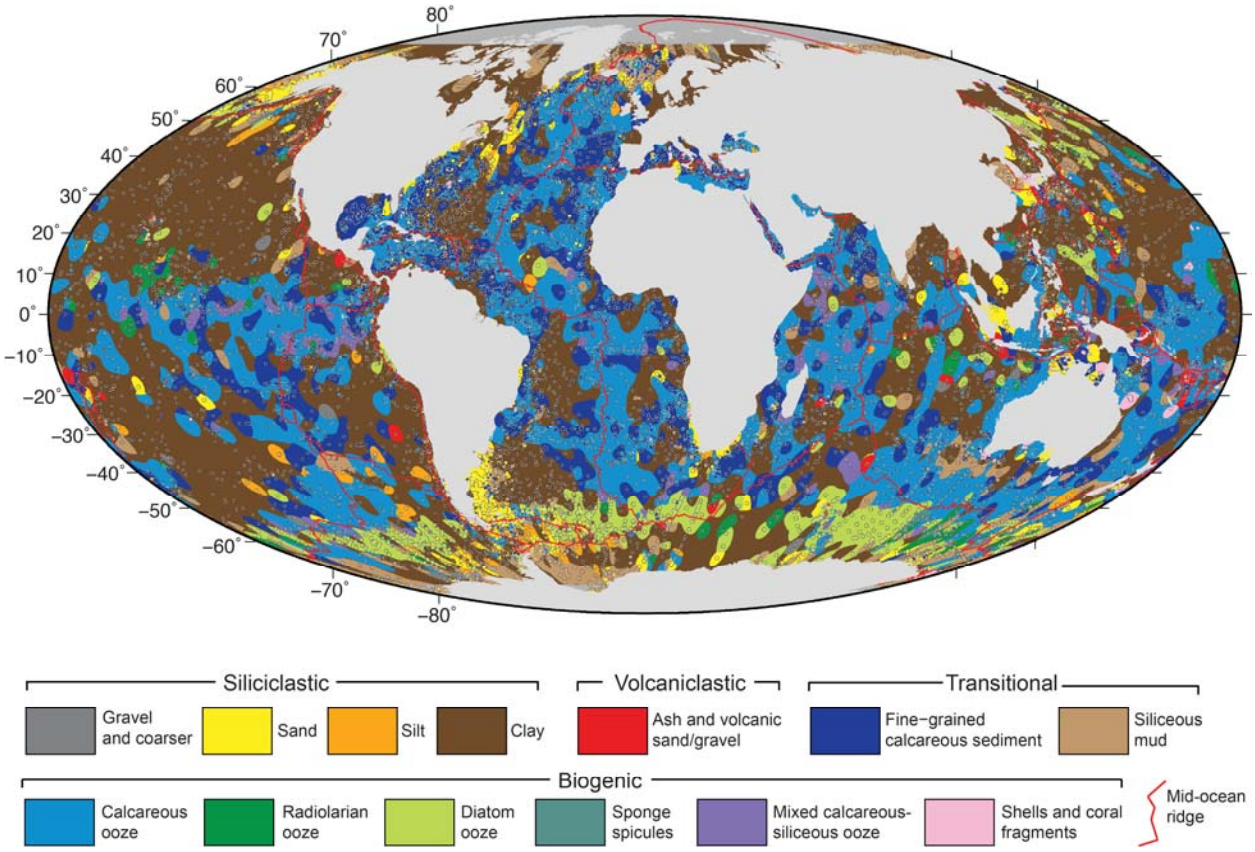

Figure DR4A. Gridded seafloor lithology map for the world's ocean with lithology-coded data points (n =14,399) superimposed. Circles with black-white outlines indicate a match between the gridded lithology and the sample point. Minor mismatching is highlighted by colored sample points, which in most cases are closely related to the gridded lithology (e.g., fine-grained calcareous sediment and calcareous oozes). Mollweide equal-area projection. The gridded data are available for download from: ftp://ftp.earthbyte.org/papers/Dutkiewicz_etal_seafloor_lithology/.

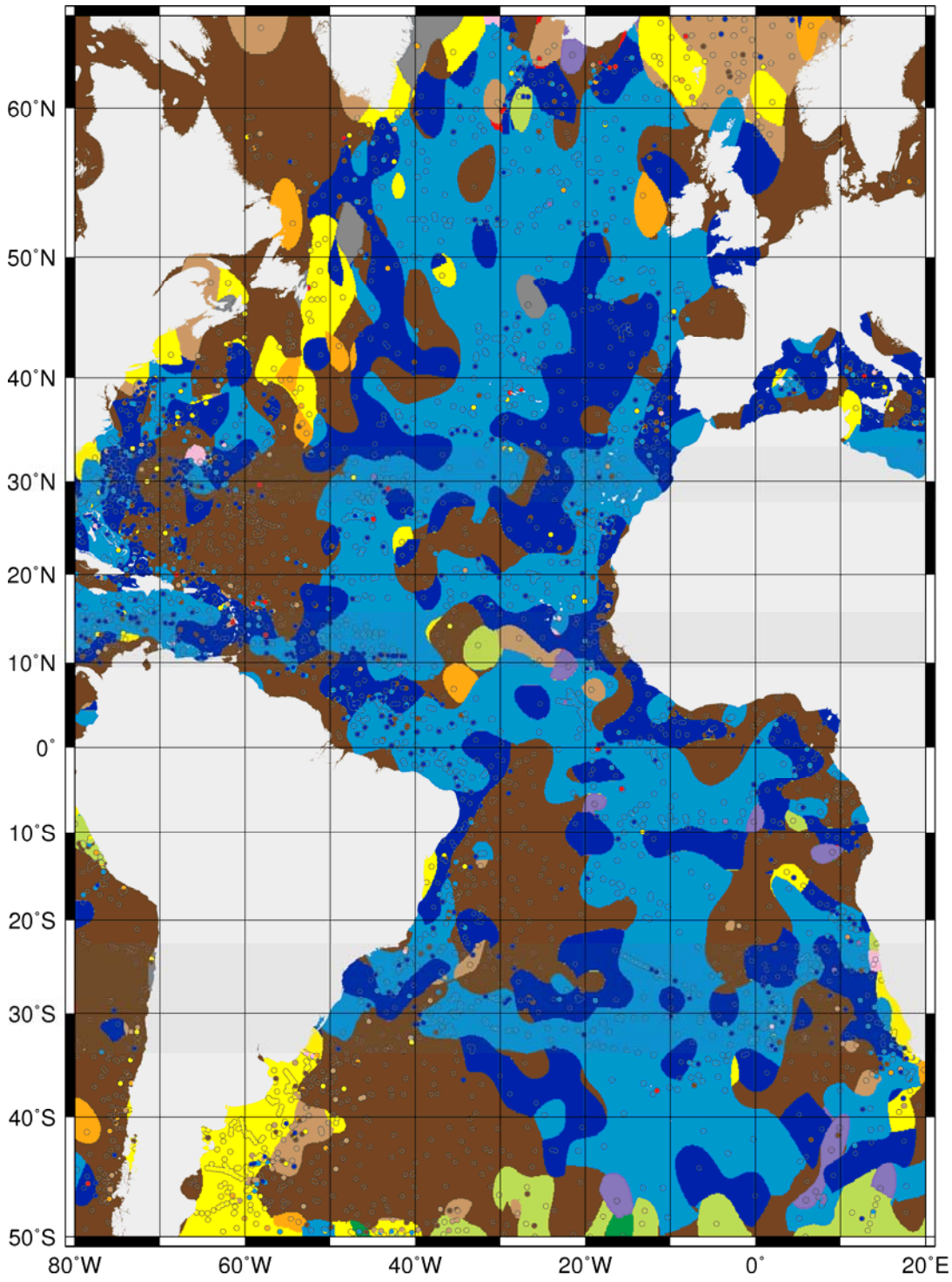

Figure DR4B. Gridded seafloor lithology map for the Atlantic Ocean with lithology-coded data points superimposed. Circles with black-white outlines indicate a match between the gridded lithology and the sample point. Minor mismatching is highlighted by colored sample points, which in most cases are closely related to the gridded lithology (e.g., fine-grained calcareous sediment and calcareous oozes). Mercator projection. Legend is the same as in Figure DR4A.

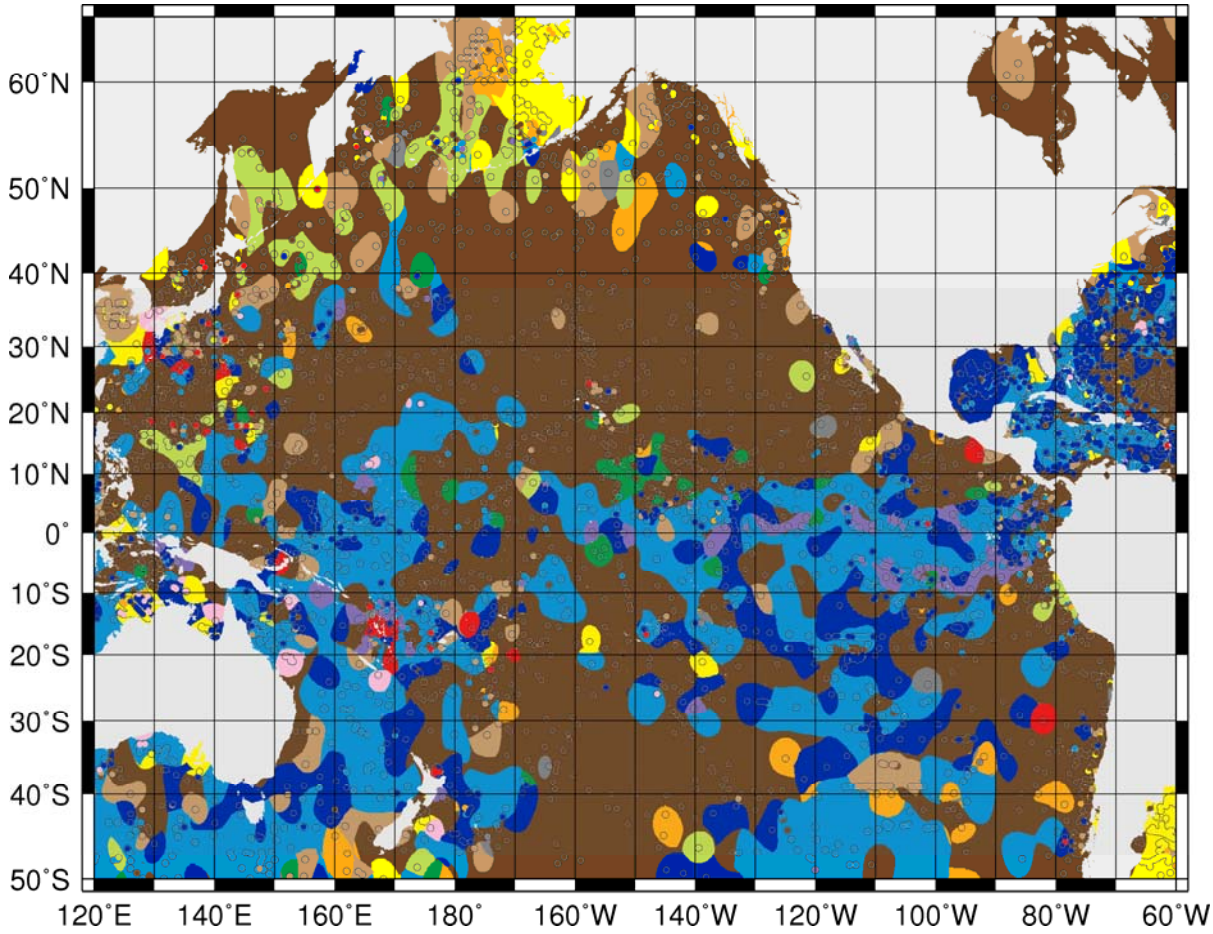

Figure DR4C. Gridded seafloor lithology map centered on the Pacific Ocean. Circles with black-white outlines indicate a match between the gridded lithology and the sample point. Minor mismatching is highlighted by colored sample points, which in most cases are closely related to the gridded lithology (e.g., fine-grained calcareous sediment and calcareous oozes). Mercator projection. Legend is the same as in Figure DR4A.

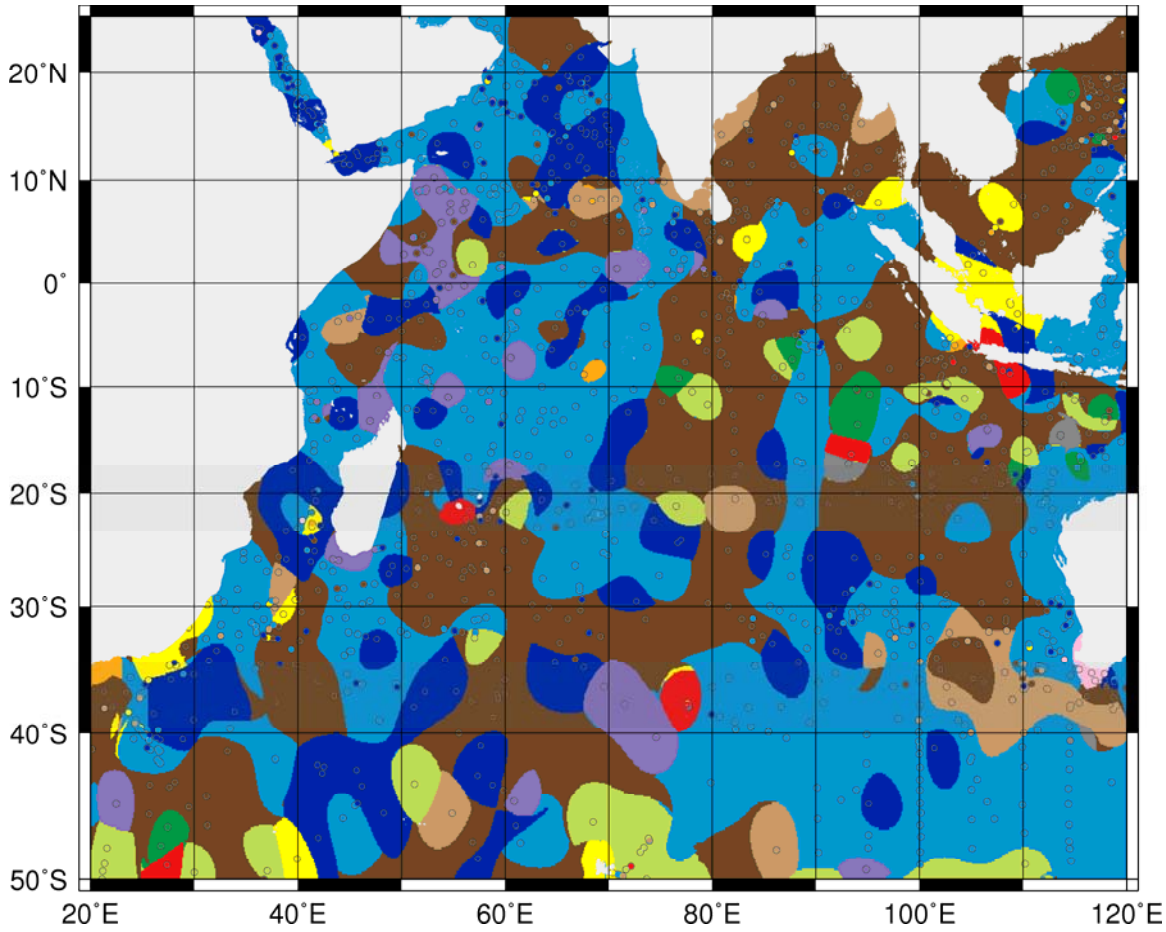

Figure DR4D. Gridded seafloor lithology map for the Indian Ocean. Circles with black-white outlines indicate a match between the gridded lithology and the sample point. Minor mismatching is highlighted by colored sample points, which in most cases are closely related to the gridded lithology (e.g., fine-grained calcareous sediment and calcareous oozes). Mercator projection. Legend is the same as in Figure DR4A.

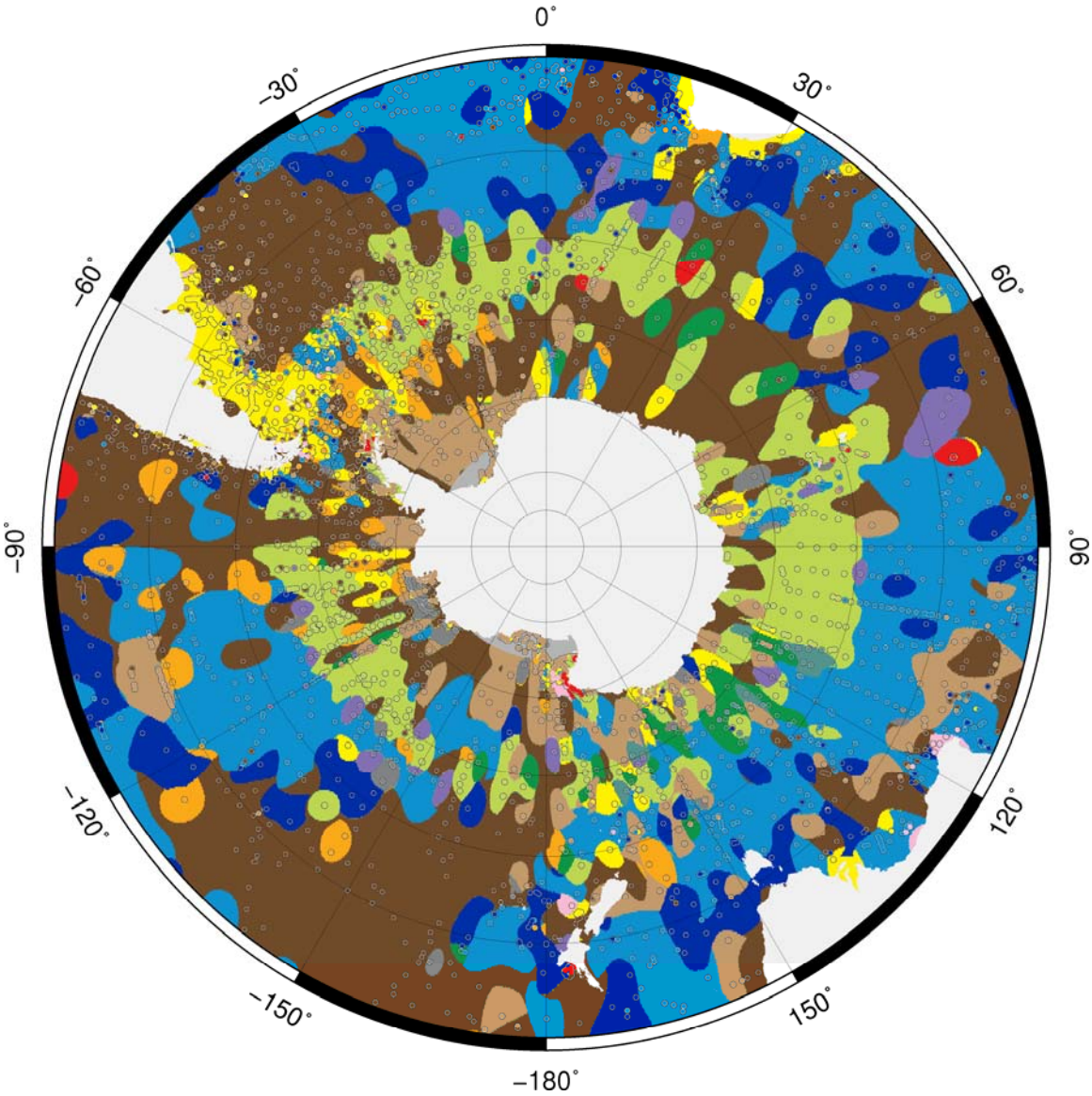

Figure DR4E. Gridded seafloor lithology map for the Southern Ocean. Circles with black-white outlines indicate a match between the gridded lithology and the sample point. Minor mismatching is highlighted by colored sample points, which in most cases are closely related to the gridded lithology (e.g., fine-grained calcareous sediment and calcareous oozes). Mercator projection. Legend is the same as in Figure DR4A.

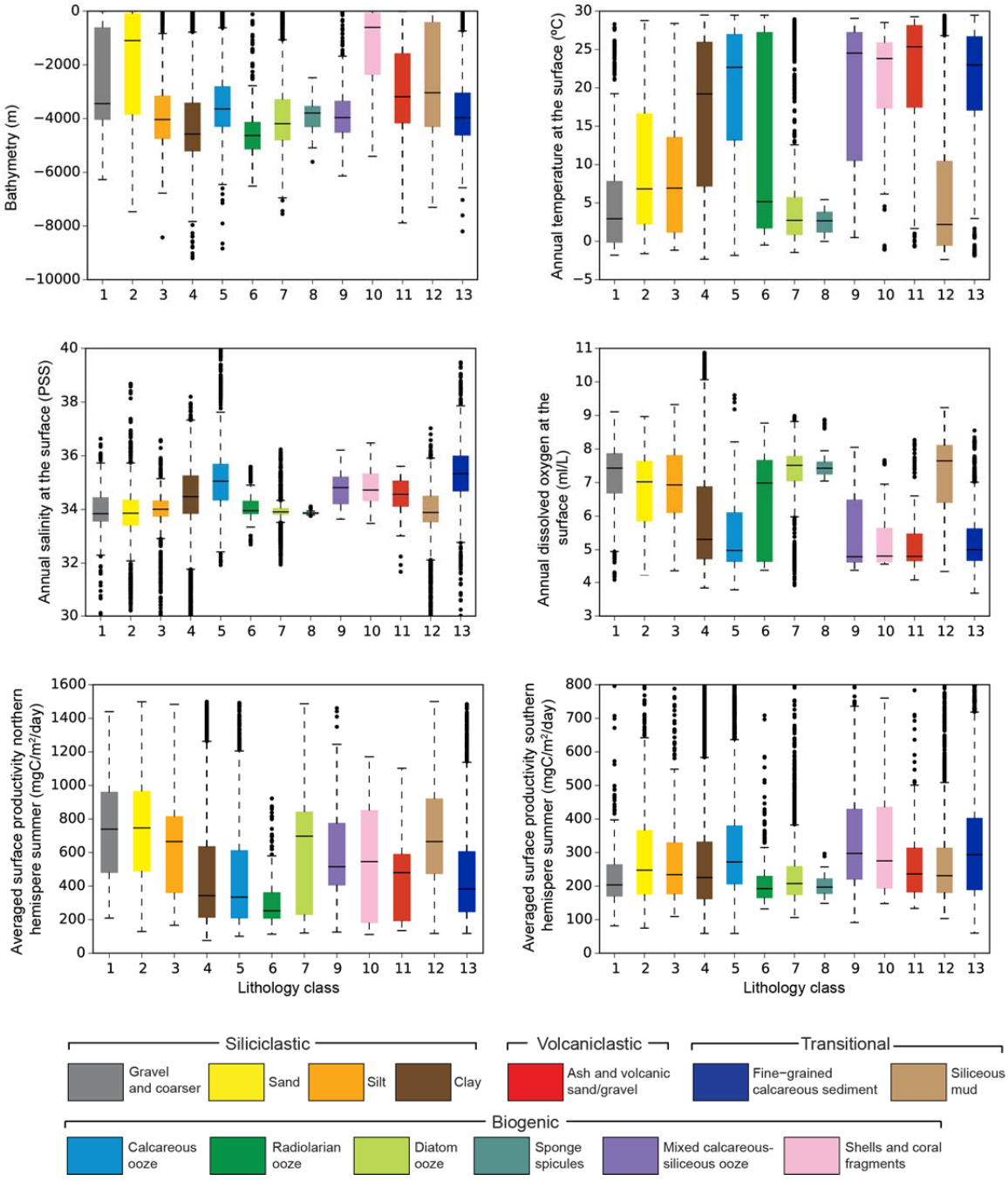

Figure DR5. Box plots of lithology classes versus various oceanographic parameters. Lithology classes are linked to numbers as follows: 1 – gravel, 2 – sand, 3 – silt, 4 – clay, 5 – calcareous ooze, 6 – radiolarian ooze, 7 – diatom ooze, 8 – sponge spicules, 9 – mixed ooze, 10 – shell and coral fragments, 11 – ash and volcanic sand/gravel, 12 – siliceous mud, 13 – fine-grained calcareous sediment. Black dots indicate sample outliers. See section on oceanographic datasets for description and links to source material.

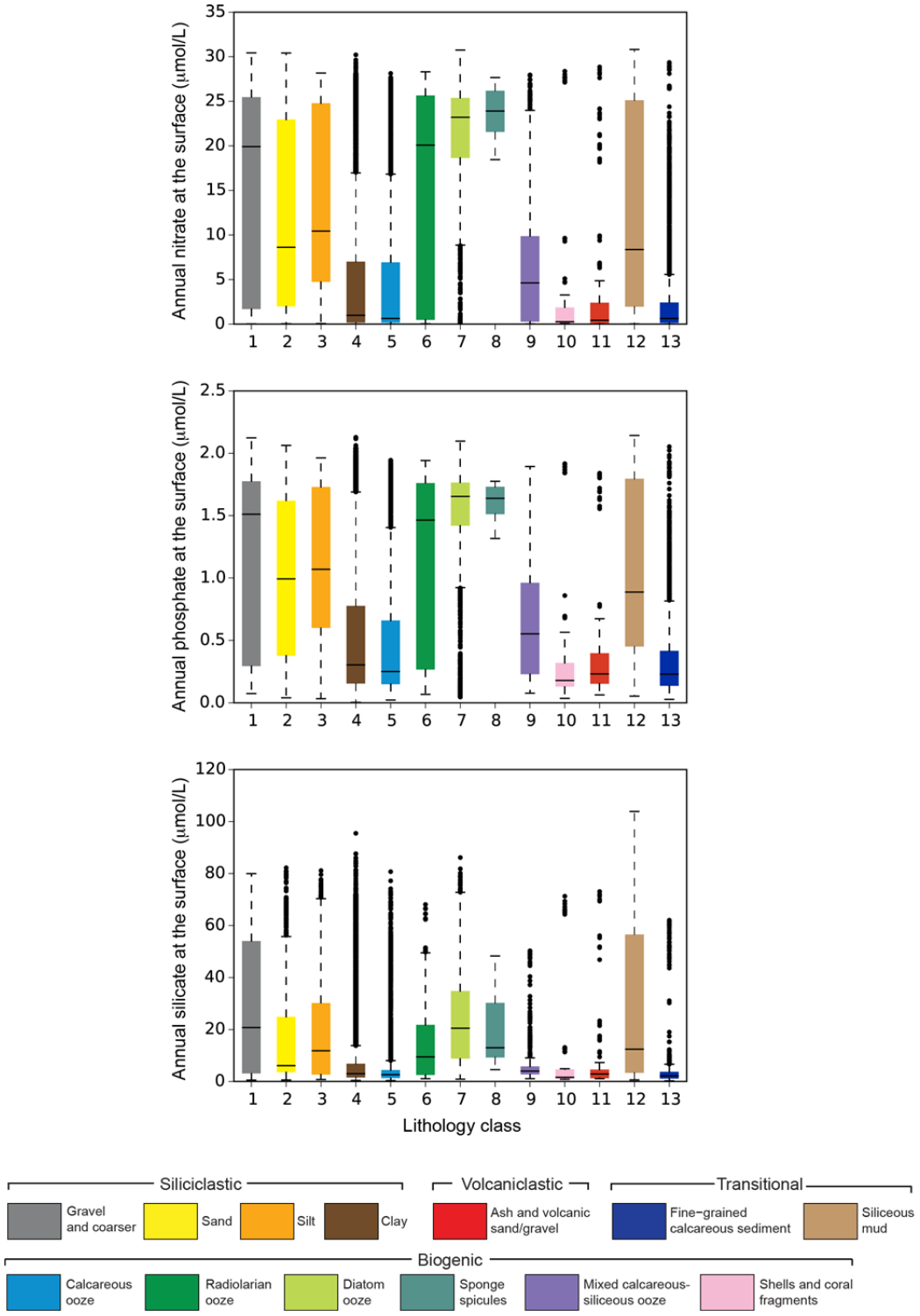

Figure DR6. Box plots of lithology classes versus various oceanographic parameters. Lithology classes are linked to numbers as in Figure DR4. Black dots indicate sample outliers. See section on oceanographic datasets for description and links to source material.

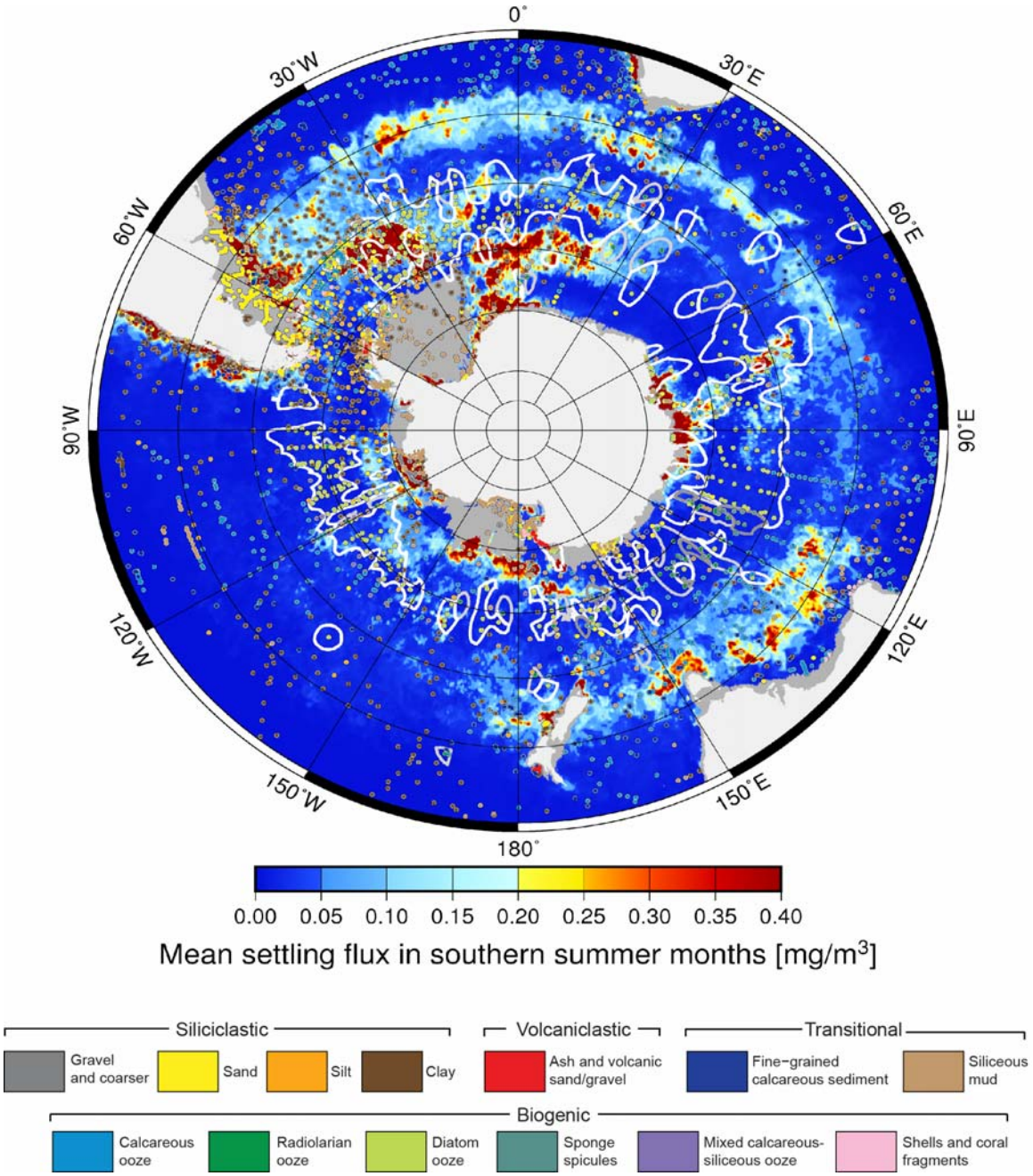

Figure DR7. Areas of biosiliceous sediments and lithology-coded surface sediment sample locations superimposed on austral summer average of diatom chlorophyll concentrations (mg/m^3) for the period 2003-2013 from the model of Soppa et al. (2014). Areas of diatom oozes, radiolarian oozes and sponge spicules are outlined in white, light grey and dark grey, respectively. Stereographic projection, latitude in 10° intervals.

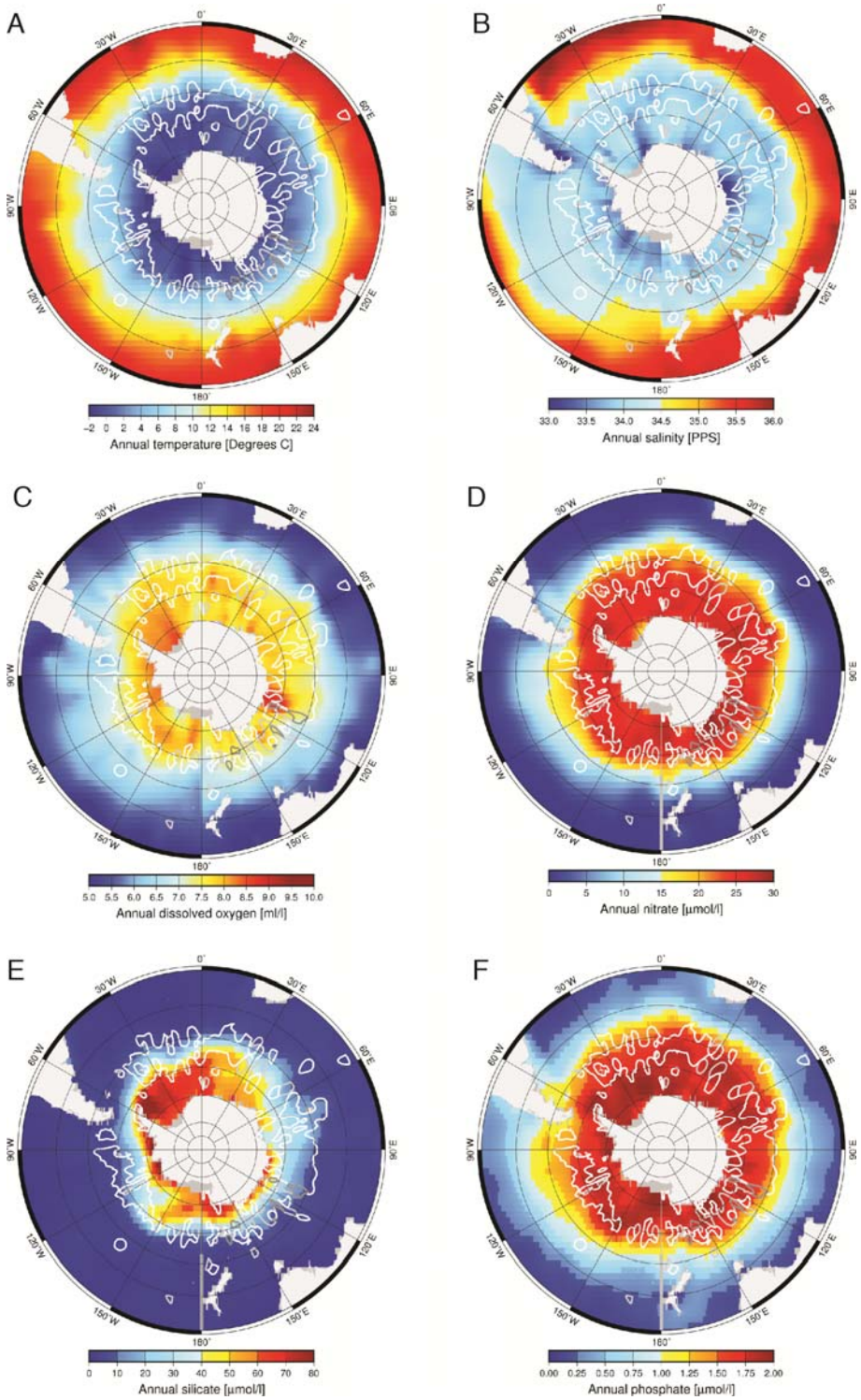

Figure DR8. Biosiliceous oozes superimposed on maps of A) annual sea-surface temperature, B) annual sea-surface salinity, C) annual dissolved oxygen, D) annual sea-surface dissolved nitrate, E) annual sea-surface dissolved silicate and F) annual sea-surface dissolved phosphate (Antonov et al., 2010; Garcia et al., 2010a; Garcia et al., 2010b; Locarnini et al., 2010). Stereographic projection, latitude in 10° intervals. Datasets downloaded from http://www.nodc.noaa.gov/OC5/WOA09/woa09data.html.

Table DR1. Distribution of main sediment types in major oceans (Arctic excluded due to poor sample coverage). Ocean area calculations, average salinities, temperatures and carbonate ion concentrations for surface waters from Feely et al. (2009). An example of similar calculations based on earlier hand-drawn maps can be found in Anderson (1988).

Ocean	Salinity (g/kg)	Temp. (°C)	Carbonate Ion (µmol kg^{1})	Clay (%)	Calc. ooze (%)	Fine-grained calc. sediment (%)	Rad. ooze (%)	Diatom Ooze (%)	Mixed ooze (%)	Other (%)*
North Atlantic 90°W to 20°E 65°N to 20°N and 80°W to 10°E 20°N to 0°	35.64 ± 1.37	19.6 ± 7.3	223 ± 34	27	36	27	< 1	<1	< 1	8
South Atlantic 70°W to 20°E 0° to 40°S	36.02 ± 0.79	22.5 ± 3.7	237 ± 22	34	39	21	< 1	< 1	1	4
North Pacific 120°E to 100°W 59.5°N to 20°N and 120°E to 80°W 20°N to 0°N	34.05 ± 0.86	20.8 ± 8.1	208 ± 38	62	16	5	3	4	1	9
South Pacific 120°E to 70°W 0° to 40°S	35.29 ± 0.55	23.3 ± 4.3	223 ± 25	43	29	15	1	1	3	9
North Indian 20°E to 120°E 0° to 24.5°N	34.72 ± 1.57	28.1 ± 0.8	244 ± 12	40	33	13	1	1	5	8
South Indian 20°E to 120°E 0° to 40°S	35.10 ± 0.47	23.5 ± 4.3	227 ± 19	33	38	14	2	3	3	7
Southern Ocean South of 40°S	34.78 ± 0.94	16.7 ± 10.5	193 ± 54	29	21	6	3	19	2	20

*Siliciclastic sediment (gravel, sand, silt, mud), shells, volcaniclastic sediment.

Table DR2. The range of variation (1QR) of key oceanographic parameters for major deep-sea lithologies. Based on box plots in Figs DR4 and DR5.

Lithology	Clay	Calcareous ooze	Radiolarian ooze	Diatom ooze	Mixed ooze
Bathymetry (m)	3431-5198	2818-4286	4144-5126	3300-4791	3359-4504
Annual temperature at the surface (°C)	7.2-25.9	13.2-26.9	1.7-27.2	0.9-5.7	10.5-27.2
Annual salinity at the surface (PSS)	33.79-35.21	34.35-35.68	33.85-34.31	33.83-34.03	34.22-35.20
Annual dissolved oxygen at the surface (ml/L)	4.74-6.87	4.65-6.10	4.65-7.66	7.06-7.78	4.64-6.48
Surface productivity northern hemisphere summer (mgC/m^2/day)	215-634	211-611	209-360	232-840	407-773
Surface productivity southern hemisphere summer (mgC/m^2/day)	163-331	207-379	166-229	175-258	221-429
Annual nitrate at the surface (µmol/L)	0.23-6.94	0.23-6.87	0.55-25.59	18.72-25.31	0.34-9.80
Annual phosphate at the surface (µmol/L)	0.16-0.77	0.15-0.66	0.27-1.76	1.42-1.76	0.23-0.96
Annual silicate at the surface (µmol/L)	1.81-6.62	1.59-4.19	2.75-21.54	9.06-34.55	2.98-5.59

REFERENCES CITED

Amante, C., and Eakins, B. W., 2009, ETOPO1 1 Arc-Minute Global Relief Model: Procedures, Data Sources and Analysis, National Geophysical Data Center, NOAA., NOAA Technical Memorandum NESDIS NGDC-24, http://www.ngdc.noaa.gov/mgg/global/global.html (November 2014).

Anderson, R. N., 1988, Marine Geology, New York, U.S.A., John Wiley & Sons, Inc., 328 p.

Antonov, J. I., Seidov, D., Boyer, T. P., Locarnini, R. A., Mishonov, A. V., Garcia, H. E., Baranova, O. K., Zweng, M. M., and Johnson, D. R., 2010, World Ocean Atlas 2009 Volume 2: Salinity. Levitus, S., ed., NOAA Atlas NESDIS 69: Washington, D.C., U.S. Gov. Printing Office, 184 p.

Barnett, P. R. O., Watson, J., and Connelly, D., 1984, A multiple corer for taking virtually undisturbed samples from shelf, bathyal and abyssal sediments: Oceanologica Acta, v. 7, no. 4, p. 399-408.

Bershad, S., and Weiss, M., 1974, Deck41 surficial seafloor sediment description database: National Geophysics Data Center NOAA, https://data.noaa.gov/dataset/deck41-surficial-seafloor-sediment-description-database (July 2014).

Boyd, P. W., and Ellwood, M. J., 2010, The biogeochemical cycle of iron in the ocean: Nature Geoscience, v. 3, no. 10, p. 675-682, doi:10.1038/ngeo964.

Cortes, C., and Vapnik, V., 1995, Support-vector networks: Machine Learning, v. 20, no. 3, p. 273-297, doi: 10.1007/BF00994018.

Curators of Marine and Lacustrine Geological Samples Consortium: Index to Marine and Lacustrine Geological Samples (IMLGS). National Geophysical Data Center, NOAA, doi:10.7289/V5H41PB8 (August-November 2014).

Denman, K. L., 2008, Climate change, ocean processes and ocean iron fertilization: Marine Ecology Progress Series, v. 364, p. 219-225, doi: 10.3354/meps07541.

Feely, R. A., Doney, S. C., and Cooley, S. R., 2009, Ocean acidification: present conditions and future changes in a high-CO_2 world: Oceanography, v. 22, no. 4, p. 37-47, doi: 10.5670/oceanog.2009.95.

Garcia, H. E., Locarnini, R. A., Boyer, T. P., Antonov, J. I., Baranova, O. K., Zweng, M. M., and Johnson, D. R., 2010a, World Ocean Atlas 2009 Volume 3: Dissolved Oxygen, Apparent Oxygen Utilization, and Oxygen Saturation. Levitus, S., ed., NOAA Atlas NESDIS 70: Washington, D.C., U.S. Gov. Printing Office, 344 p.

Garcia, H. E., Locarnini, R. A., Boyer, T. P., Antonov, J. I., Zweng, M. M., Baranova, O. K., and Johnson, D. R., 2010b, World Ocean Atlas 2009, Volume 4: Nutrients (phosphate, nitrate, and silicate). Levitus, S., ed., NOAA Atlas NESDIS 71: Washington, D.C., U.S. Gov. Printing Office, 398 p.

Hutchins, D. A., and Bruland, K. W., 1998, Iron-limited diatom growth and Si:N uptake ratios in a coastal upwelling regime: Nature, v. 393, no. 6685, p. 561-564, doi: doi:10.1038/31203.

Jickells, T. D., An, Z. S., Andersen, K. K., Baker, A. R., Bergametti, G., Brooks, N., Cao, J. J., Boyd, P. W., Duce, R. A., and Hunter, K. A., 2005, Global iron connections between desert dust, ocean biogeochemistry, and climate: Science, v. 308, no. 5718, p. 67-71, doi: 10.1126/science.1105959.

Jutzeler, M., White, J. D. L., Talling, P. J., McCanta, M., Morgan, S., Le Friant, A., and Ishizuka, O., 2014, Coring disturbances in IODP piston cores with implications for offshore record of volcanic events and the Missoula megafloods: Geochemistry, Geophysics, Geosystems, v. 15, no. 9, p. 3572-3590, doi: 10.1002/2014GC005447.

Liaw, A., and Wiener, M., 2002, Classification and regression by randomForest: R News, v. 2, no. 3, p. 18-22.

Locarnini, R. A., Mishonov, A. V., Antonov, J. I., Boyer, T. P., Garcia, H. E., Baranova, O. K., Zweng, M. M., and Johnson, D. R., 2010, World Ocean Atlas 2009, Volume 1: Temperature. Levitus, S., ed., NOAA Atlas NESDIS 68: Washington, D.C., p. 184.

Moore, J. K., and Braucher, O., 2008, Sedimentary and mineral dust sources of dissolved iron to the world ocean: Biogeosciences, v. 5, no. 3, doi: http://dx.doi.org/10.5194/bg-5-631-2008.

Passlow, V., Rogis, J., Hancock, A., Hemer, M., Glenn, K., and Habib, A., 2005, Final Report: National Marine Sediments Database and Seafloor Characteristics Project. Geoscience Australia, Canberra, Record 2005/008, http://www.ga.gov.au/oracle/mars/ (September-November 2014).

Scholle, P. A., Arthur, M. A., and Ekdale, A. A., 1983, Pelagic environment, *in* Scholle, P. A., Bebout, D. G., and Moore, C. H., eds., Carbonate Depositional Environments, American Association of Petroleum Geologists Memoir 33, p. 619–691.

Skinner, L. C., and McCave, I. N., 2003, Analysis and modelling of gravity-and piston coring based on soil mechanics: Marine Geology, v. 199, no. 1, p. 181-204, doi:10.1016/S0025-3227(03)00127-0.

Soppa, M. A., Hirata, T., Silva, B., Dinter, T., Peeken, I., Wiegmann, S., and Bracher, A., 2014, Global retrieval of diatom abundance based on phytoplankton pigments and satellite data: Remote Sensing, v. 6, no. 10, p. 10,089-010,106, doi: 10.3390/rs61010089.

Stow, D. A. V., and Aksu, A. E., 1978, Disturbances in soft sediments due to piston coring: Marine Geology, v. 28, no. 1, p. 135-144, doi:10.1016/0025-3227(78)90101-9.

Strzepek, R. F., and Harrison, P. J., 2004, Photosynthetic architecture differs in coastal and oceanic diatoms: Nature, v. 431, no. 7009, p. 689-692, doi: 10.1038/nature02954.

Trujillo, A. P., and Thurman, H. V., 2014, Essentials of Oceanography, New Jersey, Prentice Hall, 608 p.

Wessel, P., and Chandler, M. T., 2011, The spatial and temporal distribution of marine geophysical surveys: Acta Geophysica, v. 59, no. 1, p. 55-71, doi: 10.2478/s11600-010-0038-1.